Journal of Power Sources 196 (2011) 5293–5298

Contents lists available at ScienceDirect

Journal of Power Sources

journal homepage: www.elsevier.com/locate/jpowsour

Reconstruction of limited computed tomography data of fuel cell components using Direct Iterative Reconstruction of Computed Tomography Trajectories

Axel Lange[a,*], Andreas Kupsch[a], Manfred P. Hentschel[a], Ingo Manke[b], Nikolay Kardjilov[b], Tobias Arlt[b], Roman Grothausmann[b]

[a] BAM Federal Institute for Materials Research and Testing, 12200 Berlin, Germany
[b] HZB Helmholtz-Zentrum Berlin GmbH, Hahn-Meitner-Platz 1, 14109 Berlin, Germany

ARTICLE INFO

Article history:
Received 3 August 2010
Received in revised form 27 October 2010
Accepted 29 October 2010
Available online 11 November 2010

Keywords:
PEM fuel cell
Neutron computed tomography
Electron tomography
Reconstruction algorithm
Water management
Catalyst

ABSTRACT

CT (computed tomography) reconstructions of fuel cell components of a yet unrivaled spatial resolution and quality are presented. This is achieved by application of the novel DIRECTT (Direct Iterative Reconstruction of Computed Tomography Trajectories) algorithm. We focus on two different key issues which essentially rule the fuel cell's durability on different length scales and physical interactions. On the resolution scale of some 100 μm agglomerations of condensed water in flow-field channels are detected by means of quasi-*in situ* neutron CT (after operation). Five orders of magnitude below nanometer sized Ru catalyst particles on carbon black support are visualized by electron tomography. Both types of experiments are especially adapted to the type of material involved but they are accompanied by severe deviations from ideal CT measuring conditions, as well. In order to overcome the tremendous reconstruction artifacts of standard algorithms, we employ DIRECTT which is described in detail. Comparisons of DIRECTT reconstructions to the conventional filtered back projection, prove the significant improvements in both experimental methods.

1. Introduction

For a more detailed understanding of polymer electrolyte membrane fuel cells (PEMFC) very different information about their functional components have to be obtained. This refers to structural details and ageing behavior which have impact on their operation and durability [1]. The most direct way is visualization in 3 dimensions. Computed tomography (CT) is a suitable tool for non-destructive investigations of the spatially resolved "density" information from micrometers down to the nanometer scale. Different issues of interest require sensing tools adapted to the respective spatial resolution and contrast scale to be resolved.

The fuel cell's water management is of special interest since it determines the gas flux (reactants) in the flow-field channels, the degree of humidity in the gas diffusion layer (GDL) and the proton exchange membrane, as well as critical points of corrosion [2]. Neutrons are selected for imaging water agglomerates since they provide a rather high absorption contrast in relation to the other materials [3]. Strictly speaking, the contrast does not arise from real absorption but from scattering effects of the hydrogen core (proton). Here, we characterize the feasibility of neutron CT in order to distinguish water droplets at anode and cathode.

The basic fuel cell function of power generation, i.e. the electrochemical reaction of oxygen and hydrogen, is catalyzed by very small metallic particles. Here, electron tomography is utilized to image nanometer sized Ru catalyst particles with the highest precision possible in order to estimate their free (reactive) surface which rules the actual reaction rate. The outstanding feature of electron tomography technique is its unique spatial resolution in the nanometer range. Its first and most popular applications originate from molecular biology where functional groups of biological cell structures are visualized. However, electron tomography represents a major challenge to the robustness of reconstruction algorithms (away from standard routines) since the measured raw data is a unique combination of restrictions (see experimental) which have led to unavoidable strong artifacts in previous attempts when standard reconstruction algorithms were applied.

Several CT studies regarding specific aspects of fuel cells are known from the literature. High resolution X-ray CT using advanced X-ray optics was applied to image the three-dimensional (3D) microstructure of solid oxides in SOFC [4–6]. X-ray microtomography was used for imaging the gasdiffusion layer's fibre structure [7,8]. Neutron tomography studies aimed at elucidating the water management in complete PEMFC [9,10]. A very recent paper employs X-ray (synchrotron) tomography to visualize the water distribution and formation in the GDL and flow field channels of a specially designed PEMFC [11].

* Corresponding author. Tel.: +49 30 81043667; fax: +49 30 81041837.
E-mail address: axel.lange@bam.de (A. Lange).

0378-7753/$ – see front matter © 2010 Elsevier B.V. All rights reserved.
doi:10.1016/j.jpowsour.2010.10.106

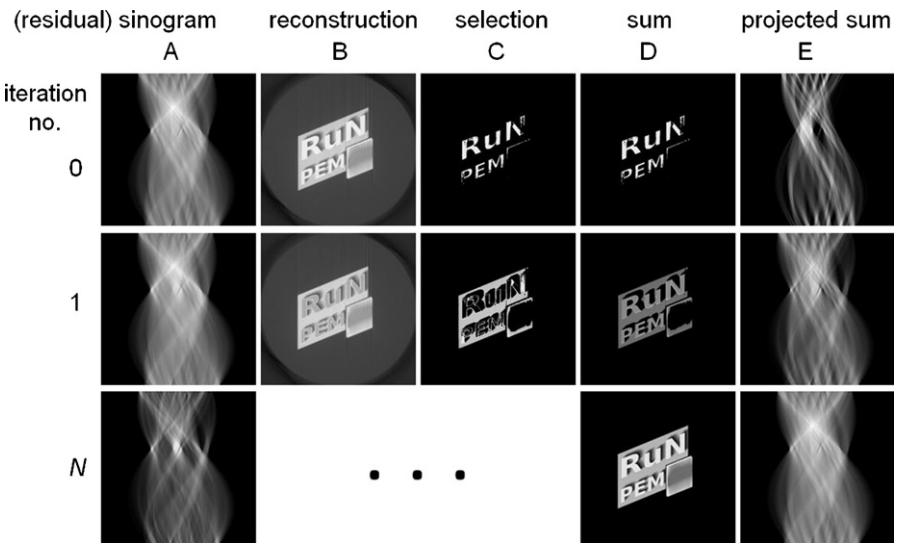

Fig. 1. The DIRECTT reconstruction principle by matrix plots. The (measured) sinogram (A) is reconstructed (B), a percentage of B is selected (C) and put into a partial reconstruction sum (D) which is projected again (E). The difference A–E is the input for the next iteration cycle until the projected sinogram (E*N*) converges towards the initial data (A0).

2. Reconstruction algorithm DIRECTT

The DIRECTT [12] algorithm represents a promising alternative to conventional reconstruction algorithms such as FBP (filtered back projection) or ART (algebraic reconstruction technique) [13]. Several successful applications and model calculations have been reported elsewhere [12,14]. At the current state of computation there are numerous refined program versions arranged for the requirements of very specific tasks such as bad raw data (regarding geometry, intensity, background) or severely limited datasets (deviating from ideal CT conditions). Here we explain the basic ideas and steps of the algorithm.

The iterative philosophy of DIRECTT is schematically displayed in Fig. 1. The algorithm is applicable to parallel as well as fan or cone beam geometry of projections. Here we study parallel beam projections. Fig. 1 is consists of matrix plots, and in the following we refer to the matrix entries (letter number) to describe the single steps of reconstruction.

We start with a so-called density sinogram (A0) which is the usual experimental input after intensity normalization (actually intensity is the measured quantity) and logarithmic conversion according to Lambert–Beer's law of attenuation. In Fig. 1 the horizontal axis of the sinograms represents a detector line while the vertical axis corresponds to the projection angle. Here we use computed projection data of the related project logo. This corresponds to the Radon transform [15] which is achieved by integration of attenuation coefficients along the beam direction under different angles of sample rotation. The given density sinogram can optionally be filtered along the detector direction. This is helpful to avoid artifact formation equivalent to the effects of an unfiltered back projection.

Demanding that each element of the reconstruction array corresponds to exactly one sinusoidal trajectory of the sinogram integral, the values for *all possible trajectories* are computed and put into the reconstruction array (B0). The DIRECTT algorithm selects pixels, i.e. area elements corresponding to trajectories of dominant weight ranking within a predefined top percentage of all trajectory weights for an update of the reconstruction (C0). The selected fraction is then weighted with a pre-defined factor and added to the partial reconstruction sum (D0) obtained in the previous step (which is zero in the first cycle).

An intriguing feature of DIRECTT refers to the possibility to adapt the filter function for trajectories evaluations of specific interest such as mass or contrast. The weights of all possible trajectories (corresponding to integer reconstruction positions) are computed by averaging along the respective traces within the optionally filtered sinogram. This involves interpolation between neighboring sinogram pixels corresponding to different detector elements. This is a substantial difference to FBP, where interpolation is performed in Fourier space (fast FBP) or in the backprojection step after the sinogram has been (inversely) Fourier transformed and filtered (real space FBP).

The projection E0 (Radon transform) of the reconstruction array (i.e. a computed sinogram) is then subtracted from the original data set (A0). The obtained residual sinogram (A1 = A0 – E0), containing trajectories of the remaining elements is subject to the same procedure in the subsequent iteration steps. Now the partial reconstruction sum D1 is calculated from D0 + C1, or in general Dx = Dx – 1 + Cx, where x is the number of iterations. This is continued until a pre-selected criterion of convergence is reached. Under ideal conditions the residual sinogram converges to zero which means that the measured (or simulated sinogram A0) is identical to the computed projection EN of the last partial sum DN. Therefore the reconstructed structure corresponds to the spatial density distribution of the projected sample.

The overall procedure corresponds to an iterative Radon transform. In contrast to FBP there is no integral computation along the line detector (including limited sampling due to its element size) but an optional oversampling along the numerous projection angles. One of DIRECTT's unique characteristics is its very precise projection of reconstruction elements taking into account their actual size and shape which is essential for enhanced spatial resolution. That is, reconstruction pixels are considered as a set of densely packed elements instead of being (circularly smeared) point functions only. Hence, all previously described calculations are performed based on squared area elements in a Cartesian matrix.

DIRECTT is of particular interest when the focus is on reconstruction of finely structured details or on precise location of reconstructed elements rather than on computing time. In contrast to FBP, the DIRECTT procedure does not treat each (detector) projection individually by filtering of any kind. Instead the entire

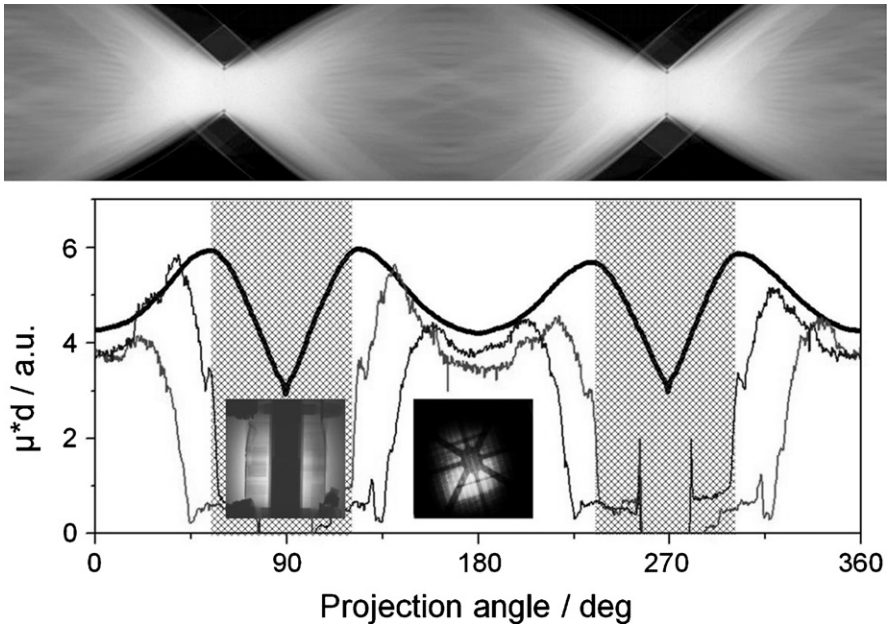

Fig. 2. Selected neutron CT density sinogram of threefold fuel cell stack (top); bottom: graphs of horizontal cumulative cross section (bold line) and linear cross sections at the detector edges (thin lines).

trajectory of a reconstruction element is considered over all projection angles. In contrast to ART, DIRECTT does not modify all reconstruction elements simultaneously.

3. Experimental

3.1. Neutron CT

Neutron tomography experiments have been performed at beamline CONRAD at Helmholtz Centre Berlin (HZB, research reactor BER II). A complete threefold fuel cell stack (incl. metal housing and supply lines) was run on site and investigated in two states: immediately after operation and 30 min later, i.e. in a quasi-stationary state (as described in [10]). The cell stack was subject to a full rotation through a 360 deg sector. 1000 single projections were recorded using a LiF flat panel detector (2048 × 2048 pixel, 100 μm pixel size, dynamic range 14 bit). Additionally, 10 flat field and dark field images were collected for the purpose of data correction.

Fig. 2, top displays an arbitrarily chosen sinogram. A sinogram is obtained from a fixed detector line (perpendicular to the rotation axis) at varying angles from a pile of projection images. Fig. 2, bottom shows the according cumulative cross section along the projection angle (fat black line in the graph below). Two orthogonal single projections at 0 deg (or 180 deg; the cell is irradiated perpendicular to the single cells) and 90 deg (irradiation parallel to the cells) are inserted. Ideal CT conditions require that the projected mass is a conserved quantity under all projection angles. As to be seen from the right insert the fuel cell is only partially projected under 0 and 180 deg (and neighboring sections). For further rotation the projected mass increases sinusoidal. When the entire sample is projected on the detector (see the left insert) a constant level of the integrated density (mass) should be expected. But because of very high absorption the disadvantageous aspect ratio causes nonlinear phase dependent attenuation. Therefore only the angular section outside the shaded region is used for the reconstructions.

An even more severe problem is implied by the large neutron aperture which amounts to some centimeters and results to inherently un-sharp projection images. This effect will be designated as 'smearing' and will turn out to be a function of the sample-detector-distance: the larger distance between sample and detector the more blurred is the obtained image. Basic calculations how to properly take into account a position dependent blurring to the reconstruction algorithm have been given [16]. A first approach aims at computing the smearing in the projection part of the iterative DIRECTT algorithm and neglecting it in the reconstruction part.

Tracing single sinusoidal trajectories (of marked objects) reveals a rotation axis which is inclined by approximately 1.3 deg with respect to the Cartesian detector coordinates. Thus, planar sinograms are oblique planes in projection space (i.e. the 3D image stack of projections). The planar information is separated by simple rotation of the single projections. Additionally, there are indications for axis misalignment in the direction of the (nearly parallel) beam which yields elliptical trajectories in the projection space. This mismatch cannot be corrected by pure data pre-processing but is a challenge for experimental alignment.

3.2. Electron tomography

Electron microscopic projections of catalysts on carbon black support have been performed *ex situ* in a Zeiss Libra® Microscope. The bright field images (in zero loss modus) are recorded in parallel beam geometry using 200 keV electrons. The actual detector resolution used here is 0.26 nm. Since none of the state-of-the-art manipulators can warrant sufficient precision in the nanometer range the technique suffers from an inherently unstable rotation axis. The measurements are performed on samples positioned on copper grids with a thin carbon foil containing gold markers. In order to have available the possibility of re-orientation of fluctuating single projections spherical gold markers are introduced to the measured volume.

Due to the sample holder's size (relative to the magnetic pole shoe distance) a full rotation of the sample is impossible, resulting in an *integral Limited View* problem. The measured angular section typically amounts to 140 deg. Because of the high electron beam brilliance local material degradations cannot be excluded. Thus, the recording time per projection (about 90 s) has to be kept as short

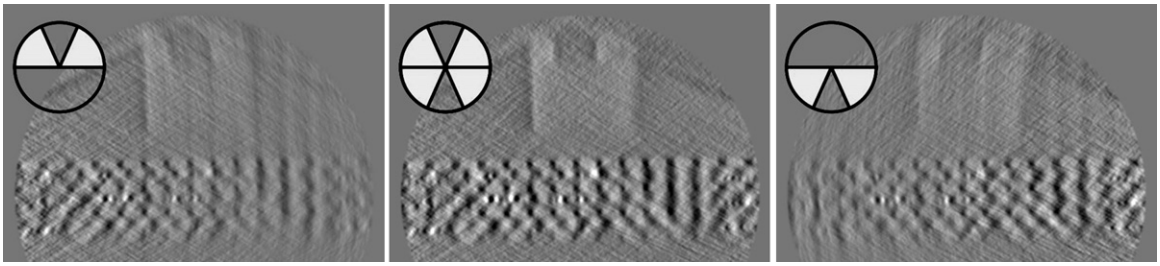

Fig. 3. Neutron CT reconstructions of transversal section of the threefold fuel cell; left and right: separate reconstructions of the two 180 deg sectors of the sinogram applying a distance related linear ramp factor in direction of each projection; middle: combination of both sectors.

as possible. The total tomographic measurement comprises merely 143 projections, i.e. with respect to the detector size (1550 pixel per line) the reconstruction suffers from a tremendously underdetermined *Few Angles* problem.

The sample (incl. Au markers) is much larger than the projected cross section, i.e. volume elements near the edge of the reconstructed region are not projected at all rotation angles and, worse, the integral mass is not conserved. This corresponds to the well-known *region of interest* (ROI) problem which hampers the empirical determination of the exact axis position since tracking the centre of gravity as a function of phase is pointless. However, knowing the axis position with the highest precision possible is of the utmost significance for the achievable reconstruction quality.

High density volume elements (Au markers, catalyst particles) are nearly opaque. The as-measured intensity is out of the valid dynamic range. As a result, the reconstructed array exhibits intense streak artifacts, since the actually penetrated lengths of the absorbing objects cannot be converted to meaningful values of the respective attenuation coefficients. Thus for the concealed partial volume a partial *phase dependent Limited View* problem results.

From the projected sector and the number of projections a mean angular increment of 1 deg is derived. However in the electron microscope the sample rotation can only be pre-selected at an accuracy of about 0.2 deg. The resulting sequence of *non-equidistant projection angles* is created by alignment and rectification of the single projections. Therefore the application of an arbitrary list of projection angles has been inserted to the DIRECTT reconstruction program in order be more precise.

4. Results

4.1. Water agglomerations in flow-fields

Part of the experimental drawbacks of neutron radiographs which refer to the phase dependent integral attenuation and the suppression of artifacts due to incomplete trajectories of projected elements (ROI) have not been overcome significantly by iterative DIRECTT reconstructions and did not justify the required additional computing time.

However, computation of the position dependent smearing of projections (due to the large aperture) yields significantly improvements. It is applied to the projection part of iterations exclusively as desmearing by deconvolution of the reconstructions would not provide a position dependent procedure [7]. Analogously to the magnification function in cone beam geometry, the smear width increases as a function of the sample's detector distance. In order to get a quantitative measure of the smearing function calibration measurements using a thin Gd foil have been performed. In the result we obtain a smear width calibration as a second order polynomial dependency on the detector distance including a 4 pixel offset (according to inherent detector smearing). On the other hand the smear width is no function of the lateral position.

Although 180 deg parallel beam data sets generally contain all information necessary for reconstruction, the full rotation data is required for the position dependent iterative smearing procedure in order to perform de-smearing after all, thus improving the reconstruction quality. Fig. 3 illustrates the successful application of the position dependent de-smearing by simply weighting the amplitudes as ramp functions along the direction of projection at the example of 180 deg sections of the sinogram (as sketched in the inserts), in which due regions (close to the detector) are favored by 'sharp' projection, respectively.

Comparing reconstructions of complete data sets an unambiguous advantage of the DIRECTT algorithm using the position dependent smearing is obvious. This is illustrated at the example of the middle cathode in Fig. 4 (perpendicular to the reconstructed slices), where the differences are very clearly. The water droplets are localized very well in the DIRECTT reconstruction but poorly in filtered back-projection.

As to be expected the more significant water indications (judging from a contrast point of view) are found at the cathode sites (where the protons migrate, i.e. where the water is formed). In the FBP the cathode structures are partially superimposed by neighboring anodes (Fig. 4, crossing channels). Obviously the determination of the condensed water concentrations at the different electrodes has been improved by the DIRECTT reconstructions.

4.2. Nanometer resolved catalyst particles

As outlined in Section 3.2 the non-equidistant angular sequence of electron tomographic projections has been applied. Two indications confirm the advantages over approximated increments: the projected trajectories of the gold markers are much more sinusoidal and the reconstruction quality increases. This includes both localized details as well as integral criteria such as weight and variance of the residual sinogram.

The reconstruction of the rather limited raw data set by standard FBP results is very disappointing images. Careful geometry corrections are required (e.g. precise axis position) and an intensity threshold (strong absorbers) in each case. Neglecting such data pre-processing results in reconstructions dominated by streak artifacts which conceal the structure of interest (Fig. 5, FBP). Moreover, these adjustments are a pre-requisite to enable the iteration.

As a result of the simultaneous occurrence of strong (gold) absorbers and the ROI problem large masses (high densities) 'from outside' (not reconstructed) density produce strong artifacts inside the ROI. Within DIRECTT the 'disturbing' mass can be suppressed by extending the reconstruction array and thus localizing it outside the ROI. This is only possible as of another advantage of DIRECTT: the geometrically true evaluation of incomplete trajectories of mass elements from outside the ROI.

The quality differences for imaging the few nanometer catalyst particles by different reconstruction algorithms are demonstrated in Fig. 5. At the example of an arbitrarily chosen detail the FBP of the raw data provides mainly artifacts. SIRT, the commonly used

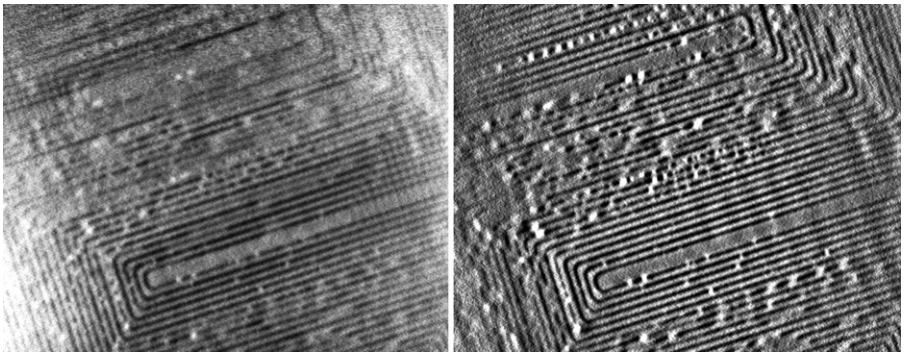

Fig. 4. Comparison of FBP filtered back-projection (left) and DIRECTT (right) reconstructions at the middle cathode plane: different contrasts and improved resolutions (perceptibility) of water droplets.

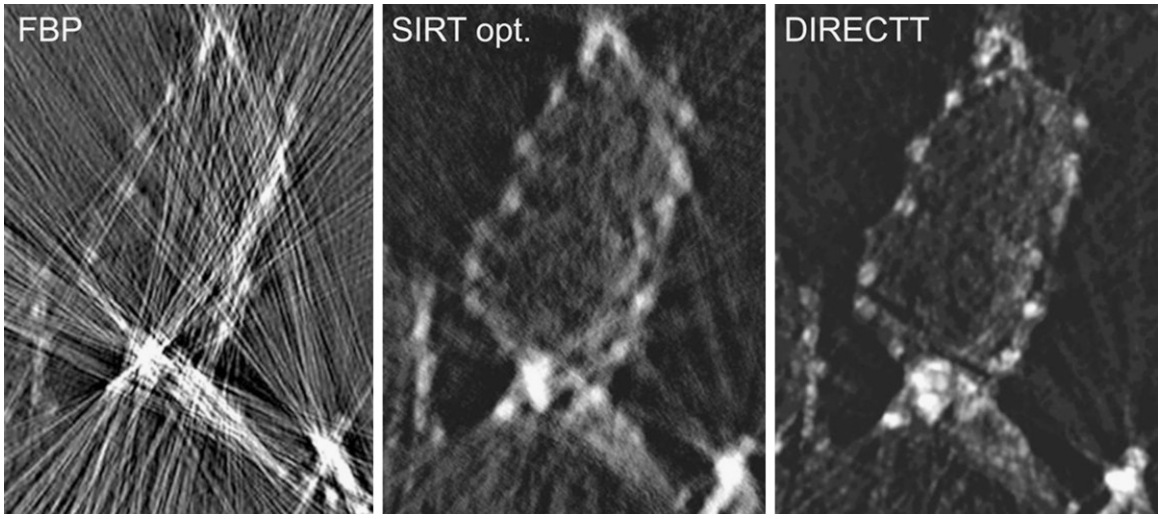

Fig. 5. Quality differences of different reconstruction algorithms as revealed by imaging properties of catalyst particles on selected carbon black support (reconstruction detail).

algorithm for electron tomography, an iterative ART procedure performs better when appropriate data preprocessing is applied. The higher quality of the DIRECTT reconstruction is obvious (Fig. 5, right), although the required computing time is two orders of magnitude shorter.

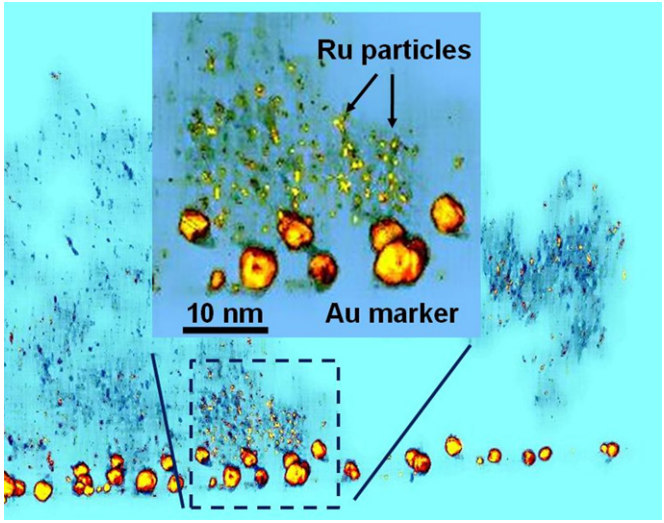

Fig. 6. 3D visualization of Ru catalyst nanoparticles and zoomed detail at about 1 nm spatial resolution; dominant 3–8 nm Au markers on cloudy carbon black supports.

Beyond the 2D details of Fig. 5 the 3D visualization of Fig. 6 gives an impression of the relative sizes and the catalyst particle arrangement on the membrane and the carbon supports. Only such precise results permits advanced data analysis which aim at the estimation of the catalysts free surface. This includes the individual ellipsoidal particle deformations and the determination of the catalyst fraction embedded in carbon.

5. Conclusion

The unique tomographic algorithm DIRECTT has been applied to solve difficult reconstruction tasks regarding fuel cell components. It copes with aperture smearing effects of neutron CT and resolves separately the water agglomerates at fuel cell cathode and anode sites. In case of the simultaneous occurrence of numerous restrictions inherent to electron tomography it provides advantages over the other relevant algorithms. Beyond the application to fuel cell components the reconstruction of any restricted tomographic data set by DIRECTT is expected to yield improved results compared to the state of the art provided that proper data preprocessing is applicable or precise measurements are given.

Acknowledgements

Funding by the German Federal Ministry of Education and Research (BMBF) under grant numbers 03SF0324 and 03MS607D is gratefully acknowledged.

References

[1] Handbook of Fuel Cells—Fundamentals, Technology and Applications, John Wiley & Sons, Chichester, 2003.
[2] C. Hartnig, R. Kuhn, P. Krüger, I. Manke, N. Kardjilov, J. Goebbels, B.R. Müller, H. Riesemeier, MP Mater. Test. 50 (2008) 609–614.
[3] I. Manke, C. Hartnig, N. Kardjilov, A. Hilger, A. Lange, A. Kupsch, J. Banhart, MP Mater. Test. 51 (2009) 219–226.
[4] J.R. Izzo, A.S. Joshi, K.N. Grew, W.K.S. Chiu, A. Tkachuk, S.H. Wang, Y. Wenbing, J. Electrochem. Soc. 155 (2008) B504–B508.
[5] A. Tkachuk, F. Duewer, H.T. Cui, M. Feser, S. Wang, W.B. Yun, Z. Kristallogr. 222 (2007) 650–655.
[6] S. Griesser, G. Buchinger, T. Raab, D.P. Claassen, D. Meissner, J. Fuel Cell Sci. Technol. 4 (2007) 84–87.
[7] A. Pfrang, D. Veyret, F. Sieker, G. Tsotridis, Int. J. Hydrogen Energy 35 (2010) 3751–3757.
[8] P. Rama, Y. Liu, R. Chen, H. Ostadl, K. Jiang, X.X. Zhang, R. Fisher, M. Jeschke, J. Fuel Cell Sci. Technol. 7 (2010) 031015.
[9] I. Sakata, T. Ueda, H. Murakawa, K. Sugimoto, H. Asano, N. Takenaka, R. Yasuda, T. Tomura, M. Shiozawa, Nucl. Instrum. Methods A 605 (2009) 131–133.
[10] I. Manke, Ch. Hartnig, M. Grünerbel, J. Kaczerowski, W. Lehnert, N. Kardjilov, A. Hilger, W. Treimer, M. Strobl, J. Banhart, Appl. Phys. Lett. 90 (2007) 184101.
[11] Ph. Krüger, H. Markötter, J. Haußmann, M. Klages, T. Arlt, J. Banhart, Ch. Hartnig, I. Manke, J. Scholta, J. Power Sources 196 (2011) 5250–5255.
[12] A. Lange, M.P. Hentschel, A. Kupsch, MP Mater. Test. 50 (2008) 272–277.
[13] A.C. Kak, M. Slaney, Principles of Computerized Tomographic Imaging, Classics in Applied Mathematics, SIAM (2001), vol. 33, IEEE Press, New York, 1988.
[14] A. Kupsch, A. Lange, M.P. Hentschel, Proceedings 17th World Conference on Non-Destructive Testing, 2008.
[15] J. Radon, Berichte der math.-phys. Kl. Sächsischen Gesellschaft der Wissenschaften 59 (1917) 262–277.
[16] A. Kupsch, A. Lange, M.P. Hentschel, B.R. Müller, MP Mater. Test. 52 (2010) 394–400.